Available online at www.sciencedirect.com
ScienceDirect
Remote Sensing of Environment 112 (2008) 1730–1748
Remote Sensing of Environment
www.elsevier.com/locate/rse

Detecting land cover change at the Jornada Experimental Range, New Mexico with ASTER emissivities

A.N. French [a,*], T.J. Schmugge [b], J.C. Ritchie [c], A. Hsu [c], F. Jacob [d], K. Ogawa [e]

[a] U.S. Arid Land Agricultural Research Center, USDA/ARS, 21881 N. Cardon Lane, Maricopa, AZ 85238, USA
[b] Gerald Thomas Professor of Water Resources, College of Agriculture, New Mexico State University, Las Cruces, NM 88003, USA
[c] USDA/ARS Hydrology and Remote Sensing Laboratory, Beltsville, MD 20705, USA
[d] Institute of Research for the Development, Laboratory for studies on Interactions between Soils-Agrosystems-Hydrosystems, UMR LISAH SupAgro/INRA/IRD, Montpellier, France; formerly at Remote Sensing and Land Management Laboratory, Purpan Graduate School of Agriculture, Toulouse, France
[e] School of Engineering, University of Tokyo, Japan

Received 30 November 2006; received in revised form 28 August 2007; accepted 31 August 2007

Abstract

Multispectral thermal infrared remote sensing of surface emissivities can detect and monitor long term land vegetation cover changes over arid regions. The technique is based on the link between spectral emissivities within the 8.5–9.5 μm interval and density of sparsely covered terrains. The link exists regardless of plant color, which means that it is often possible to distinguish bare soils from senescent and non-green vegetation. This capability is typically not feasible with vegetation indices. The method is demonstrated and verified using ASTER remote sensing observations between 2001 and 2003 over the Jornada Experimental Range, a semi-arid site in southern New Mexico, USA. A compilation of 27 nearly cloud-free, multispectral thermal infrared scenes revealed spatially coherent patterns of spectral emissivities decreasing at rates on the order of 3% per year with R^2 values of ~0.82. These patterns are interpreted as regions of decreased vegetation densities, a view supported by ground-based leaf area index transect data. The multi-year trend revealed by ASTER's 90-m resolution data are independently confirmed by 1-km data from Terra MODIS. Comparable NDVI images do not detect the long-term spatially coherent changes in vegetation. These results show that multispectral thermal infrared data, used in conjunction with visible and near infrared data, could be particularly valuable for monitoring land cover changes.

Keywords: ASTER; Thermal infrared; Emissivity; Jornada; MODIS; Land cover change

1. Introduction

Monitoring the spatial and temporal changes in land cover for semi-arid and arid land regions is required for hydrologists, ecologists and agronomists. Land cover information is used by hydrologists to update surface conditions affecting stream flow, infiltration and evapotranspiration (Menenti et al., 2005; Su, 2000), by agronomists for acreage and yield prediction (Fang, 1998), and by ecologists for assessing the relationships between land degradation, human activities, and global climate change (Chehbouni et al., 2000). The need for this monitoring is especially important in dry regions, since many of these are productive agricultural lands under pressure from extreme drought and population increase (Falkenmark, 1997).

Land cover change has been documented for decades over critical semi-arid regions, such as West Africa (Diouf and Lambin, 2001), in the Mediterranean Basin (El Kharraz et al., 2004), and for more than 100 years in southern New Mexico, USA (Buffington and Herbel, 1965). In the latter instance, observations have revealed large and deleterious changes where rangeland previously dominated by grass has become dominated by mesquite and creosotebush (Gibbens et al., 2006; Havstad et al., 2000).

* Corresponding author.
E-mail address: Andrew.French@ARS.USDA.GOV (A.N. French).

0034-4257/$ - see front matter © 2007 Elsevier Inc. All rights reserved.
doi:10.1016/j.rse.2007.08.020

The significance of these long-term observations, though previously recognized, has only begun to be fully appreciated by the use of remotely sensed data spanning multiple decades (Rango et al., 2005). Using frequent synoptic remote sensing observations of arid lands, especially if they were available at resolutions better than 100m, would greatly improve our ability to monitor, analyze and understand the implications of rapid land cover changes.

A common approach to monitoring land cover change compatible with the objective of long term monitoring is to collect well-calibrated vegetation index (VI) data [e.g., the normalized difference vegetation index (NDVI) and its variants]. These observations are now routinely collected at daily to bi-weekly temporal sampling and at spatial resolutions between 1 m and 1 km from sensors such as Ikonos (Dial et al., 2003), Advanced Spaceborne Thermal and Reflection radiometer (ASTER) (Yamaguchi et al., 1998), Landsat (Goward et al., 2001), the Vegetation instruments aboard Satellites Pour l'Observation de la Terre (SPOT4 and SPOT5), and MOderate-resolution Imaging Spectrometer (MODIS) (Justice and Townshend, 2002; Justice et al., 1998), each of which provides useful estimates of living, green vegetation. The relationship between vegetation indices and fractional cover and leaf area indices has been widely investigated (e.g., Gutman and Ignatov, 1998; Choudhury, 1987; Baret et al., 1995; Carlson and Ripley, 1997; Jiang et al., 2006), meaning that accurate and reliable estimates of green biomass are usually obtainable from remote sensing platforms, provided ancillary data about observational conditions and expected plant cover types are also available. Based on these established relationships, time series of VI data have been used to detect both seasonal and yearly land cover changes (Wardlow et al., 2007; Telesca and Lasaponara, 2006; Anyamba and Eastman, 1996; Justice et al., 1986; Byrne et al., 1980).

Although the vegetation index approach has demonstrated its value for land cover change monitoring, it has a frequently unmentioned shortcoming — during plant dormancy, VI values are similar to and possibly indistinguishable from bare soils. Even for indices specifically designed to minimize soil background effects, such as the Modified Soil Adjusted Vegetation Index (MSAVI) (Qi et al., 1994), the spectral inputs from red and near infrared wavelengths do not readily distinguish soils from non-green vegetation. In instances where the landscape is bare soil, the VI maps are likely representative of true conditions. But for other instances where the above-ground biomass remains during winter months, and is senescent or inactive, the resultant VI maps are not representative. For much of the year in arid lands, living plants are non-green; and discriminating them from soil, using indices such as NDVI, is difficult. When assessing vegetation cover changes over a period of years, the difficulty is particularly significant because within-season VI variabilities are just as large, or larger than, interannual VI variabilities. The difficulty is exacerbated by an inability to obtain frequent remote sensing images because of cloud cover (e.g., from Landsat) or because the spatial resolution is too coarse for areas of interest (e.g., from MODIS). Unless one can be confident that VI extremes within a plant growth cycle are captured, postulated VI trends will be biased by insufficient temporal sampling. Hence, use of VI methods to infer rates of land cover change over sparsely vegetated landscapes can be misleading.

More recent work indicates VI can be improved by incorporation of hyperspectral near infrared (NIR) data, such as in the 2.2 μm region, where cellulose and lignin absorption features appear (Bannari et al., 2006; Daughtry et al., 2005). In these ongoing studies, good discrimination between soil and vegetation appear possible using end-member analyses.

When evaluating land cover over months to years, an alternative monitoring approach does exist and is based upon spatial estimation of thermal infrared emissivities. Emissivity (ϵ_λ), a measure of thermal radiation efficiency, is defined as the ratio between actual emitted radiation (L_λ) and emitted radiation from a blackbody ($L_{\lambda,\mathrm{BB}}$) at the same temperature:

$$\epsilon_\lambda = \frac{L_\lambda}{L_{\lambda,\mathrm{BB}}} \tag{1}$$

Emissivity is the proportionality factor that distinguishes brightness temperatures from true radiometric temperatures (Norman and Becker, 1995) and is important for modeling the earth's surface energy balance. The energy balance at long wavelengths also plays a role in the ability to observe land surface emissivities:

$$L_{\mathrm{sensor}} = \epsilon L_{\mathrm{surface}} + (1-\epsilon)L\downarrow \tag{2}$$

where thermal infrared radiation (TIR) observed by a sensor (L_{sensor}) just above the surface is the weighted sum of band surface emitted radiation (L_{surface}) and band downwelling sky radiation ($L\downarrow$). Band-averaged emissivity (ϵ) and its complement are the weighting factors, which means that estimation of surface emissivity is only possible when contrast exists between (L_{surface}) and ($L\downarrow$). Emissivity is independent of temperature itself and varies spectrally according to surface composition and geometry. These latter properties make emissivity observations potentially useful for land cover characterization. Measurements at laboratory scales (Salisbury and D'Aria, 1992; Elvidge, 1988), for example, show that emissivities of soil and vegetation are commonly distinct and do not rely upon plant chlorophyll content. This makes emissivity a potential tool for discriminating soil and vegetation emissivities. At field scales, soil and vegetation can still be distinguished (Humes et al., 1994), as illustrated by observations of senescent vegetation during a 1997 study over Oklahoma (French et al., 2000). In that instance, emissivities at wavelengths between 8 and 9.5 μm were close to 1.0 for vegetation, while those for soils were ~0.91. Considering the capabilities of VI and emissivity data together, a three-way characterization of land cover is possible by distinguishing bare soils, green vegetation, and non-green vegetation.

Since 2000 an important remote sensing capability became available through the launch of the ASTER instrument in December 1999 onboard the Terra satellite. ASTER uniquely offers multispectral thermal infrared (TIR) remote sensing at moderate resolution (90 m), data unavailable elsewhere. Using ASTER's five thermal bands, land surface emissivities could be estimated in ways similar to that used by French et al. (2000) for the Oklahoma study, allowing more extensive evaluation of the land cover discrimination approach.

One such evaluation arose fortuitously from ongoing studies of a semi-arid rangeland in southern New Mexico, USA, at a research site utilizing remote sensing image data to monitor landscape structural evolution and land surface-atmosphere exchanges. The study site, known as the Jornada Experimental Range (Jornada), has been the focus of local and regional remote sensing studies since 1995. The primary theme of these studies is assessment of rangeland health, including that of vegetation land cover changes.

Vegetation cover changes at Jornada have been dramatic and occur over a wide range of time scales. Using surveys from 1858, Gibbens et al. (2006) document the transformation of the rangeland from a productive grassland to a degraded landscape dominated by shrubs in 1998. Over this 140 year span, grassland decreased from 67–98% coverage to less than 1%. Recent Jornada studies (e.g., Snyder and Tartowski, 2006) suggest too that significant vegetation changes occur at much shorter time spans, particularly at seasonal to annual scales where vegetation patterns change in complex ways in response to highly variable water availability.

The importance of Jornada for this study is that vegetation cover changes in this area have occurred at observable time scales and that related ground observations may be available to help validate changes inferred from remotely sensed emissivities. Using ASTER data over 2001–2003, consisting of 27 nearly cloud-free scenes, emissivity trends can be analyzed and compared with independently obtained observations.

Analysis and comparisons proceed in six main steps. First, emissivity retrieval approaches from the multispectral thermal infrared sensor ASTER are considered. Three different techniques are described and implemented. This is done because consensus is lacking for optimal temperature-emissivity separation and because of concerns that inferred emissivity changes could be data processing artifacts. Second, information about the Jornada setting is discussed. In the third step, the significance of the emissivity changes is considered. Here tests are employed to determine the importance of interfering effects upon emissivity retrieval precision and bias. In the fourth step, the study focus, emissivity changes observed over Jornada are described, with particular attention paid to anomalously large changes indicative of vegetation land cover degradation. Fifth, an important related issue is addressed, namely the relationship between vegetation cover and thermal emissivities. Frequently emissivity data are estimated from VI's, an approach that effectively questions the utility of emissivity observations. Here the non-equivalence of remotely sensed VI's and emissivities are shown. Sixth, the overall significance of the ASTER-Jornada study is discussed and ASTER emissivity patterns are interpreted.

2. Remote sensing estimation of emissivity

A major benefit of multispectral thermal infrared remote sensing is its ability to estimate land surface temperatures, spectral emissivities, and broadband emissivities within the TIR window. These properties are especially valuable when observed simultaneously because they help achieve land surface temperature (LST) accuracies better than 1 °C and help distinguish between different land surfaces according to soil, rock and vegetation cover (Tonooka, 2001; Gillespie et al., 1998; Hook et al., 1992, 2001). By contrast, spectral emissivity characterization is not feasible with single-window TIR, nor with most dual-window TIR instruments. Although it is true that multiple bands also cannot resolve the under-determined TIR remote sensing problem (i.e., that for N bands, there exist N+1 unknowns, namely N emissivities plus one surface temperature), they do allow objective characterization of the emissivity spectrum, an accomplishment otherwise infeasible. This makes it possible to relate spectral variations to surface composition and surface cover, as well as help improve atmospheric corrections (Tonooka, 2001).

Various approaches to estimating emissivity from multi-band TIR data exist, examples of which are discussed in Jiménez-Muñoz et al. (2006), Jacob et al. (in press), Dash et al. (2002), and Li et al. (1999). Analyses considered in this study were the Temperature-Emissivity Separation (TES, Gillespie et al., 1998) approach, the Temperature-Independent Spectral Indices (TISI, Becker and Li, 1990) approach, and the Normalized Emissivity Method (NEM, Gillespie, 1985; Kahle and Alley, 1992; Kahle et al., 1980) approach. For reasons discussed below, the primary approach used for the Jornada study was NEM. However, TES and TISI were also employed to demonstrate that results from the land cover change assessment were not contingent upon the choice of algorithm.

One of the better-known temperature and emissivity algorithms for ASTER images is TES, a procedure that resolves the under-determinacy[1] by employing an empirical functional relationship between emissivity spectral contrast and minimum emissivity (Matsunaga, 1994). With TES the minimum emissivity (ϵ_{min}) of a sample can be closely approximated by estimating the range of either absolute or relative emissivities ($\Delta\epsilon$) via the formula:

$$\epsilon_{min} = b_0 + b_1 \Delta\epsilon^{b_2} \quad (3)$$

where parameters b_0, b_1, and b_2 are derived from laboratory measurements of emissivities. For standard ASTER data products, the parameters are based on over 200 laboratory samples. For this study, the parameters used were 0.994, −0.687, and 0.737, respectively. By iteratively combining Eq. (3) with atmospherically corrected surface emitted radiance for each thermal band, the radiometric surface temperature can be separated from emissivities for each TIR band.

Based on simulation studies, Gillespie et al. (1998) show that accuracies of ±1.5 °C and ±0.015 in emissivities are possible with TES. Recent experience with ASTER and TES generally confirms this assessment, particularly for geological applications, where emissivity contrasts are large (Tonooka, 2001; Rowan et al., 2005; Rowan and Mars, 2003; Hook et al., 2005).

Due to the method's complexity, readers interested in TES implementation details should consult Gillespie et al. (1998) and the ASTER Theoretical Basis Document for the standard data product AST05.[2]

[1] The under-determination can also be resolved with multiple observations, as is done in the day-night method (Watson, 1992). That method however is highly sensitive to measurement errors, atmospheric correction errors, and co-registration of images (Mushkin et al., 2005).

[2] Available at: http://eospso.gsfc.nasa.gov/eos_homepage/for_scientists/atbd/docs/-ASTER/atbd-ast-05-08.pdf.

Table 1
Power function parameters for ASTER TIR bands according to: $L=\alpha T^n$, with spectral radiance L ($mWm^{-2}sr^{-1}\ \mu m^{-1}$) and temperature (K)

Band	$\overline{\lambda}$	α	n
10	8.2819	1.782−10	5.539
11	8.6313	6.211−10	5.323
12	9.0757	2.660−9	5.074
13	10.650	1.537−7	4.360
14	11.2812	5.462−7	4.132

$\overline{\lambda}$ is the band's central wavelength (μm).

For agricultural applications the TES procedure is less satisfactory because the land surfaces are dominated by high emissivities. In these cases, TES's differencing approach tends to underestimate emissivities and consequently overestimate land surface temperatures, particularly over gray body targets such as vegetation (Jacob et al., 2004). Potential emissivity errors can exceed 2.0%, resulting in errors of 2–3 °C. This outcome is a consequence of the method's inability to distinguish between true and apparent spectral contrast, where the latter can be due to signal noise or inaccurate atmospheric compensation. Improving temperature and emissivity retrievals for studies therefore requires alternatives to ensure that high emissivity targets remain so after the temperature-emissivity separation.

One way to achieve such a result is to utilize the normalized emissivity method (NEM, Gillespie, 1985; Kahle and Alley, 1992), an initialization procedure for TES. NEM is straightforward: a maximum spectral emissivity ϵ_{max} appropriate for the scene (0.98 is used for this Jornada study) is specified for whichever band has the maximum surface brightness temperature. Commonly this maximum temperature appears in bands sampling wavelengths between 10 and 13 μm. Once identified, the radiometric surface temperature at that band is computed, then applied to the remaining TIR bands to extract spectral emissivities.

The NEM approach of pre-specifying ϵ_{max} is not an arbitrary one and requires some judgment based on landscape context and targets of interest (Kahle and Alley, 1992). Pre-specification has a direct effect upon emissivity retrieval, where consistent selection of ϵ_{max} allows meaningful relative comparisons of emissivities between different scenes, but may cause substantial differences with respect to other temperature-emissivity separation techniques. Since ϵ_{max} is close to 1.0, sensitivity to its pre-specification is small when accounting for downwelling sky radiation [last term in Eq. (2)]. Nerry et al. (1998) show that the impact of assuming an initial emissivity while computing a downwelling radiation correction term was small, ≤0.14%. Dash et al. (2005) found yet smaller uncertainties. For combined soil and vegetated terrain, band averaged maximum emissivities are commonly within 1.5% of 0.98. Considering soil emissivity spectra from the Johns

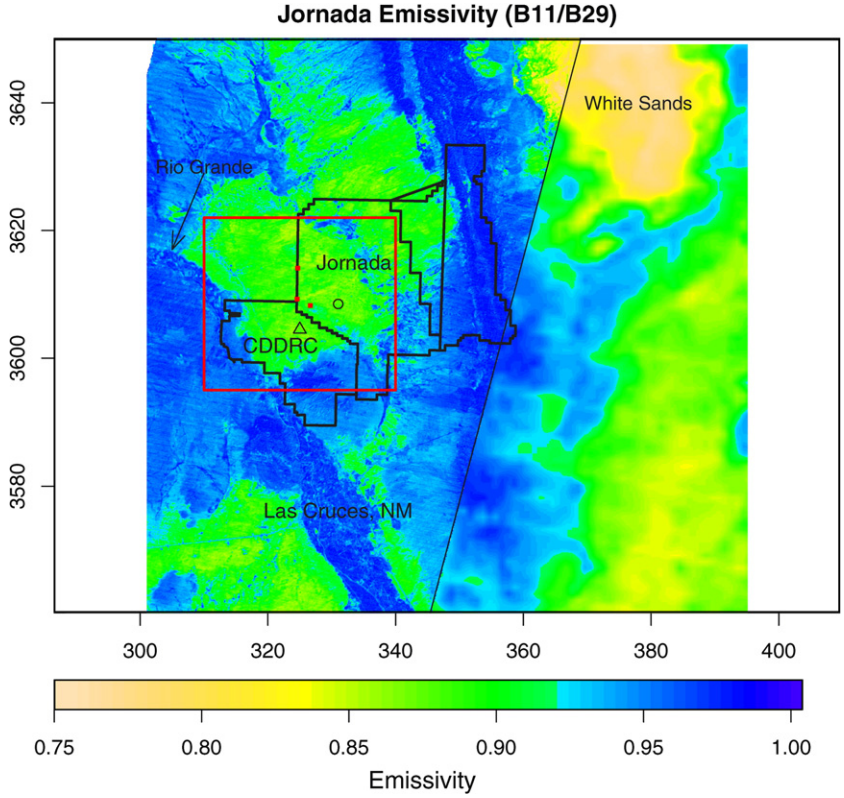

Fig. 1. Jornada regional overview of emissivities in the 8.5–8.8 μm TIR window. The display is a composite of ASTER band 11 emissivities to the left of the bold line and MODIS band 29 emissivities to the right. Axes are annotated with UTM zone 13 coordinates in kilometers. Red squares indicate LAI transect sites. The open triangle and circle indicate sites denoted as 'Degraded' and 'Reference', respectively. The region has strong emissivity differences, where the Jornada is dominated by lower emissivities (<0.9) and is characterized by sandy soils, while agricultural lands in the Las Cruces area are dominated by higher emissivities (>0.95). The White Sands region has even lower emissivities (~0.8) because of its gypsum-covered surface.

Hopkins collection within the ASTER spectral library (Salisbury and D'Aria, 1992; Jet Propulsion Laboratory, 2001), 39 of 41 samples (95%) had $\epsilon_{max}>=0.965$ somewhere in the TIR window. For this library set, 38 of the 41 had the maximum emissivity located in either ASTER band 13 or 14 (10.25–11.65 μm), while 3 were associated with the shorter wavelength ASTER band 10 (8.125–8.475 μm). No maximum values were found in ASTER bands 11 or 12 (respectively, 8.475–8.825 and 8.925–9.275 μm). At more typical remote sensing scales (e.g., 90 m for ASTER), vegetation is viewed as a canopy rather than as individual leaves and multi-scattering effects would increase maximum emissivities to over 0.99 and reduce the variability of maximum emissivities (Fuchs and Tanner, 1966, 1968; Sutherland and Bartholic, 1977; Norman et al., 1995; Palluconi et al., 1990; Zhang and Smith, 1990).

Another method that can overcome the low ϵ_{max} problem is TISI (Becker and Li, 1990), a technique that computes relative emissivities ($TISI_{i,j}$) from power-scaled brightness temperatures:

$$\mathrm{TISI}_{i,j} = \left[\frac{T_i}{T_j}\right]^{n_i} \tag{4}$$

where T_i and T_j are atmospherically corrected brightness temperatures for spectral channels i and j. The exponent n_i can be determined from a least squares analysis:

$$L_i \sim \alpha_i T_i^{n_i} \tag{5}$$

where channel spectral radiance is L_i ($\mathrm{mWm^{-2}sr^{-1}\ \mu m^{-1}}$) and radiometric temperature for a channel is T_i (K).

Table 1 lists the best-fit terms for Eq. (5), considering ASTER channels 10–14. TISI values are nearly independent of land surface temperature, which means that their uncertainties can potentially be low, given accurate atmospheric corrections. However, TISI values are non-unique, dependent upon the chosen bands, and indicate emissivity ratios, as discussed by Becker and Li (1990). To retrieve emissivities themselves, further observations or additional assumptions are needed. In the former case, nighttime shortwave infrared data are suitable (Petitcolin and Vermote, 2002), but in this study, such data at 90 m spatial scales are not available. In the latter case, a reference channel emissivity can be used in the same way as for the NEM approach.

In summary, remote sensing estimation of emissivity at Jornada can be achieved in several ways, three of which are considered here. None can be accomplished in the current context without underlying assumptions. These include assumptions about spectral emissivity contrast and the existence of an accurate emissivity reference channel.

3. The Jornada experiment

The Jornada Experimental Range (Jornada) research area is a semi-arid rangeland in southern New Mexico, 30 km northeast of the city of Las Cruces and 40 km west of White Sands (Fig. 1). The core study sites are within the Jornada Experimental Range, a US Department of Agriculture research site since 1912 to study effective management of grazingland. Jornada is also a Long Term Ecological Research (LTER) site (http://jornada-www.nmsu.edu), a collaborative research program established by the National Science Foundation in 1980 to support research on long-term ecological phenomena in the United States (http://lternet.edu/). South of Jornada is the New Mexico State University Ranch, also known as the Chihuahuan Desert Rangeland Research Center (CDDRC, http://spectre.nmsu.edu/dept/welcome.html?t=cdrr). Typical vegetation at Jornada includes grass and shrub areas. The principal grasses include black grama [*Bouteloua eriopoda* (Torr.) Torr.], mesa dropseed [*Sporobolus flexuosus* (Thurb. Ex Vasey) Rydb.], and three awn [*Aristida purpurea* Nutt. and *Aristida pansa* Wooton and Standl.]. Shrubs and suffrutescents are commonly C3 plants and include honey mesquite [*Prosopsis glandulosa* Torr.], fourwing saltbush [*Atriplex canescens* (Pursh) Nutt.], broom snakeweed [*Gutierrezia sarothrae* (Pursh) Britton and Rusby], and soaptree yucca [*Yucca elata* (Engelm.)].

Jornada ground sites were selected to represent grass, grass–shrub ecotone (transition), and shrub (mesquite) ecosystems. The transition site has vegetation components of both the grass and shrub sites. Dunes are developing at the transition site but are usually less than 1m in height. Honey mesquite on coppice dunes dominates the shrub site. Bare soil with almost no vegetation dominates the areas between these coppice dunes. The sites will be referred to as Grass (32.5981° N, 106.8471° W), Transition (32.6068° N, 106.8695° W) and Mesquite (32.6507° N, 106.8695° W) in this paper. As previously noted, rangeland at Jornada and throughout the US Southwest has degraded

Table 2
Selected ASTER/MODIS overpass dates

Count	Day	Month	Year	DOY	Cumulative Days (since 1/1/2001)	Δ Days
1	12	Feb	2001	43	42	–
2	12	May	2001	132	131	89
3	22	Jul	2001	203	202	71
4	17	Sep	2001	260	259	57
5	19	Oct	2001	292	291	32
6	11	Nov	2001	315	314	23
7	20	Nov	2001	324	323	9
8	23	Jan	2002	23	387	64
9	8	Feb	2002	39	403	16
10	24	Feb	2002	55	419	16
11	3	Mar	2002	62	426	7
12	15	May	2002	135	499	73
13	31	May	2002	151	515	16
14	23	Jun	2002	174	538	23
15	10	Aug	2002	222	586	48
16	26	Aug	2002	238	602	16
17	4	Sep	2002	247	611	9
18	20	Sep	2002	263	627	16
19	7	Nov	2002	311	675	48
20	23	Nov	2002	327	691	16
21	10	Jan	2003	10	739	48
22	11	Feb	2003	42	771	32
23	31	Mar	2003	90	819	48
24	18	May	2003	138	867	48
25	10	Jun	2003	161	890	23
26	7	Sep	2003	250	979	89
27	16	Oct	2003	289	1018	39

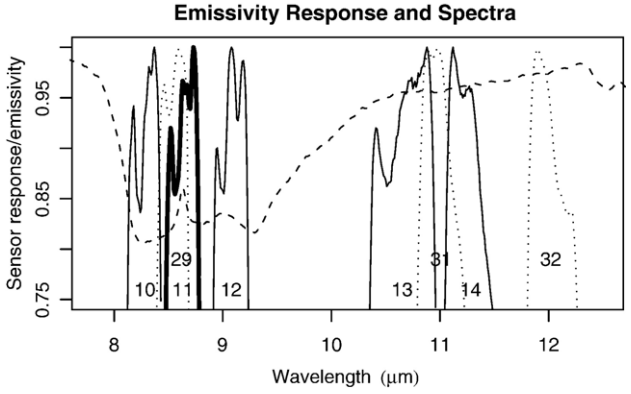

Fig. 2. Thermal band response functions for MODIS and ASTER. MODIS bands (dotted) are B29, B31, and B32, respectively left to right. ASTER bands (solid, with bold B11) are B10, B11, B12, B13, and B14. Note that MODIS B29 response is similar to ASTER B11. MODIS B31 and B32 do not have similar matches with ASTER bands B13 and B14. The dashed curve illustrates an example soil emissivity spectrum from Jornada, showing lower emissivities within the 8–9.5 μm interval.

substantially, with significant gains in mesquite/coppice dune populations at the expense of beneficial grassland.

Since 1995, semi-annual remote sensing experiments using a range of aircraft and satellite detectors have been conducted at Jornada (JORNEX) to monitor land cover changes, assess landform distributions and estimate water vapor and energy fluxes prior to and following seasonal monsoonal rainfall between June and September (Havstad et al., 2000). With the successful launch of NASA's EOS Terra satellite in December 1999, the experiments have been enhanced by dedicated observations with the ASTER sensor.

From 47 scene acquisitions, 27 mostly cloud-free images acquired between February 2001 and October 2003 were selected for processing (Table 2). To ensure the best possible analyses, all visible/near-infrared (VNIR) images were georegistered to within 15m accuracies and thermal infrared (TIR) images to within 90m accuracies using common ground control points. Estimates of spectral emissivities were done by procedures previously described in Section 2, with primary emphasis upon the NEM approach.

Since the objective of this study was to investigate the ability of emissivities to detect land cover change, analysis focused on shorter TIR wavelengths where most of the emissivity variability in soils occurs (Fig. 2). At wavelengths 10.5–12 μm, emissivity variability is small for most land cover conditions, whereas for 8–10 μm interval variations potentially range from less than 0.8 to 0.98. Not all soils exhibit this high spectral variability. Examples of low spectral variability include fine-grained, moist, and quartz-poor soils. In these circumstances, distinction between bare soils and soils covered with vegetation could be difficult. At Jornada soil emissivity variability is high, as exemplified by the dashed line in Fig. 2. Three ASTER bands sample the high-variability interval: 10, 11, and 12. Band 11 (8.475–8.825 μm) was used for this study because it is less sensitive to atmospheric correction uncertainties than Band 10 (8.125–8.475 μm) and because it did not have the anomalous gain changes of Band 12 (8.925–9.275 μm) discussed by Tonooka et al. (2003, 2005). Furthermore, Band 11 is nearly identical to MODIS band 29 (8.4–8.7 μm), allowing spectral comparisons with this coarser resolution sensor.

To ensure the best possible TIR retrievals, ASTER thermal data were calibrated using both reference radiometric database coefficients and temporally based interpolation coefficients needed to account for detector gain changes between routine updates. These interpolated values were particularly important for calibration of ASTER band 12.

To estimate vegetative cover, both remote sensing and ground measurements were used. For the remote sensing data, NDVI values were derived from ASTER bands 2 and 3N reflectances previously aggregated to 90 m. The reflectances were inferred from at-sensor radiances by using the 6S atmospheric radiative transfer model (Vermote et al., 1997) and NOAA radiosonde profile data (http://raob.fsl.noaa.gov) from Santa Teresa, NM (EPZ, 31.90° N, 106.70° W, ~75 km south of Jornada). For the ground measurements, the three sites previously mentioned (Grass, Transition, Mesquite) were used for semi-annual leaf area index (LAI) transect data. Each transect was 150 m long with LICOR LAI-2000 measurements collected at 1-meter intervals for three 30-m sections through vegetation including grass and shrubs. The measurements approximate total canopy cover, whether green or not.

To help verify ASTER emissivities at Jornada, ground collections of multiband TIR radiometric data from four sites were used (Table 3). In situ samples were acquired with a tripod-mounted 5 band CIMEL-312T instrument, while loosely-bagged soil samples were measured (hemispheric reflectance) in the laboratory using a Beckman spectrophotometer at the Jet Propulsion Laboratory, Pasadena, California (http://speclib.jpl.nasa.gov). Four of the resulting emissivity spectra were collected at the transect sites (1 at the Grass site, 1 at the Transition site, and 2 at the Mesquite site) and corresponded to quartz-bearing soils with low emissivities between 8 and 12 μm. The fifth spectrum corresponded to gypsum from the western

Table 3
Field, laboratory, and ASTER band 11 emissivities at the Grass, Transition, Mesquite and White Sands sites

Site	Source	B11 Emissivity
Grass	Cimel	0.893
	Lab	0.882
	ASTER	0.886
Transition	Cimel	0.800
	Lab	0.803
	ASTER	0.872
Mesquite	Cimel	0.718
(Bright Sand)	Lab	0.703
	ASTER	–
Mesquite	Cimel	0.847
(Dark Sand)	Lab	0.880
	ASTER	0.853
White Sands	Cimel	0.740
(Gypsum)	Lab	0.724
	ASTER	0.725

Two soil sample types were acquired at Mesquite. Data sources were in situ Cimel-312T radiometric observations and bagged surface samples for laboratory spectrophotometry.

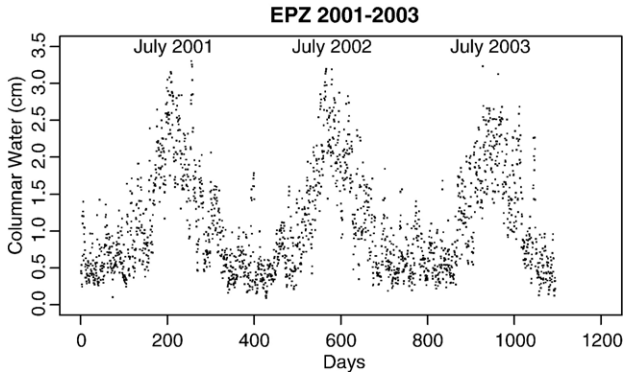

Fig. 3. Atmospheric columnar water vapor for the 2001–2003 period measured by the EPZ radiosonde. The peaks correspond to monsoonal conditions. Day to day variability, typically less than 1.0 cm, was used to estimate the uncertainties of associated atmospheric properties used for thermal infrared correction.

edge of White Sands (32.8222°N, 106.4125°W). In contrast to quartz-rich soils, gypsum has generally high emissivities (>0.96) except for 8.5–8.9 μm wavelengths, where it is strongly reflective ($\epsilon \sim 0.72$–0.74). Agreement between field, laboratory, and ASTER data are generally very good. Emissivity differences were less than 0.016 in most instances. Exceptions occurred where samples could not be collected intact (surface crusts at Mesquite) and where ASTER could not resolve spatial heterogeneities (at Transition).

4. Emissivity retrieval uncertainty

Although accurate retrieval of land surface emissivities is important, a greater concern for land cover change assessment is consistent emissivity retrieval, since it is the temporal change of emissivity that will determine the effectiveness of the analysis. When considering interfering factors for change assessment, four are critical: instrumental noise, georegistration errors, anomalously wet soils, and inaccurate atmospheric corrections. Fortunately, most of these errors for the Jornada study were small and unimportant. In particular, instrumental errors in the TIR bands were <0.4 °C (Tonooka et al., 2005). Georegistration errors were also small, <90 m, because all scenes were registered with ground control points. Considering the variability scale of vegetation at Jornada ranges between 3 and 8 m Pelgrum (2000), in conjunction with a 90 m pixel size, apparent temporal changes in emissivities due to mis-registrations were not significant. Wet soils too were rarely a problem because rainfall shortly before selected overpasses did not occur. The one exception occurred in September 2002 when rainfall was heavy shortly before overpass time. The effect of this event is discussed further in Section 5.

Since three of four critical interfering factors were not significant concerns for the Jornada study, the greatest concern for change analyses was ensuring adequate removal of atmospheric effects. Inaccurate corrections could overwhelm small emissivity changes and invalidate results. Thus, quantifying the potential effects of atmospheric correction uncertainty became important, especially when using atmospheric profiles that were not acquired at overpass times, nor co-located over Jornada.

To assess correction uncertainties, a sensitivity analysis of atmospheric profile correction was conducted using simulations. By assuming temporal variability equivalence between the profile over the radiosonde site and profiles above Jornada, and by developing relationships between the correction terms and columnar water vapor (the dominant factor affecting TIR corrections), the expected effect of uncertain TIR corrections upon emissivity could be estimated.

The tests were performed in four steps. The first step quantified variability of columnar water vapor over the Santa Teresa radiosonde site (EPZ) by considering the atmospheric database from 2001 to 2003. The second step established empirical relationships between columnar water vapor and atmospheric correction terms for each of the five ASTER TIR bands. This was done by performing simulations using MODTRAN radiative transfer code and a subset of the EPZ database. The third step generated apparent emissivities using the relationships from step 2 and the variability data obtained from step 1. Specifically, MODTRAN simulations were performed and applied to the NEM algorithm for each of the 27 ASTER scenes using radiosonde profiles and normally distributed perturbations to the correction terms. The fourth step extracted the statistical outcomes for ASTER band 11 emissivities from each site of interest.

In step one, columnar water vapor for 2159 EPZ radiosonde profiles was computed and plotted by time (Fig. 3). Water vapor amounts ranged ~0.2–3.4 cm with strong seasonal increases associated with summer monsoons. Day-to-day water vapor also varied seasonally, ranging ~25–45% of columnar water amounts. To include a wide range of realistic simulated atmospheric conditions throughout the year, the upper limit value (45%) was used for subsequent simulations.

In step two, MODTRAN runs were performed using a subset (359) of the 2001–2003 atmospheric profile database. Outputs were filtered with ASTER TIR spectral response functions,

Table 4
Coefficients to estimate ASTER TIR atmospheric correction parameters based on columnar water vapor

Band	τ			$L\uparrow$			$L\downarrow$		
i	b_0	b_1	p	b_0	b_1	p	b_0	b_1	p
10	−0.08447	−0.1859	0.7935	273.4	1117.4	0.7420	355.2	1992.2	0.7218
11	−0.07470	−0.1180	0.8247	258.4	788.8	0.7943	428.7	1325.6	0.8116
12	−0.06872	−0.0722	0.9783	244.6	557.2	0.9144	433.6	908.9	0.9439
13	−0.03421	−0.0590	1.3600	172.9	466.5	1.2782	294.2	780.4	1.2551
14	−0.02422	−0.0780	1.3178	100.9	575.2	1.2378	172.4	946.9	1.2192

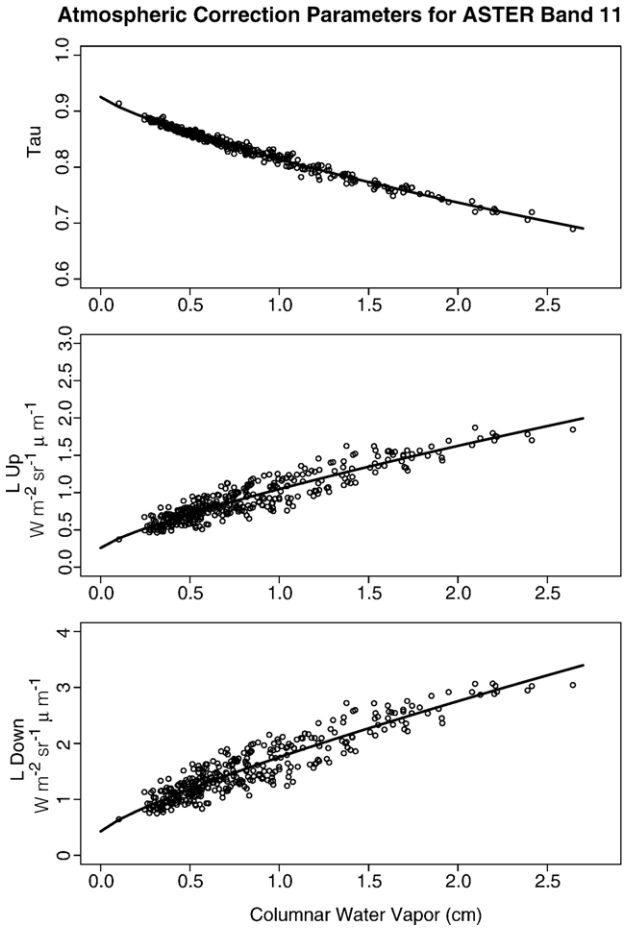

Fig. 4. Atmospheric correction terms for ASTER band 11 based on EPZ radiosonde data and MODTRAN simulations. A six-month sample of radiosonde profiles from 2001 were modeled and filtered to obtain ASTER transmissivities (top), upwelling spectral radiance (middle), and hemispherically integrated downwelling spectral radiance (bottom). Lines are empirical fits used in simulations to convert between columnar water vapor and correction terms.

modeled with power functions, and checked against the remainder of the database. The estimation functions were:

$$\tau_i = b_{0i} + \exp\left[b_{1i} w^{p_i}\right] \tag{6}$$

for atmospheric transmissivity, and:

$$L_i = b_{0i} + b_{1i} w^{p_i} \tag{7}$$

for path radiance (upwelling and downwelling). The terms b_{0i}, b_{1i}, and p_i correspond to the parameters in Table 4. w is columnar water vapor (cm). Eqs. (6) and (7) are valid for columnar water vapor amounts between 0.25cm and 2.5cm.

Graphical examples of these functions compared with MODTRAN output values are shown in Fig. 4 for ASTER band 11.

In step three, 1001 MODTRAN simulations were run using randomly generated, Gaussian distributed, τ (transmissivity), $L\uparrow$ (upwelling path radiance), and $L\downarrow$ (hemispherically integrated downwelling radiance) correction terms for each of the 27 ASTER scenes. The chosen number of simulations was based on a compromise between the need for large sample sizes and time needed for computations. Distribution plots from test runs indicated 101 simulations were insufficient, whereas output from 10001 runs were only marginally different from 1001 runs (odd numbers were used to simplify median sampling). Atmospheric corrections were done according to the atmospheric radiative transfer equation:

$$L_{\text{surface},i} = \frac{L_{\text{sensor},i} - L\uparrow_i}{\tau_i} - (1-\epsilon_i)L\downarrow_i \tag{8}$$

where $L_{\text{surface},i}$ is radiance emitted by the surface for channel i and $L_{\text{sensor},i}$ is radiance observed by the sensor. For each scene, the closest-in-time radiosonde profile was used to derive the mean value of each of the atmospheric correction terms in Eq. (8). Apparent instead of observed columnar water vapor

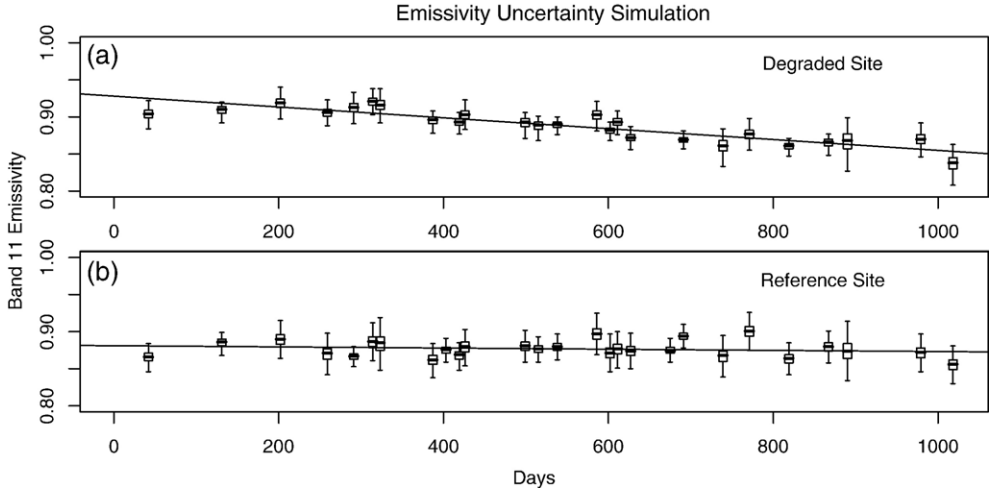

Fig. 5. Emissivity estimation uncertainty over Jornada due to atmospheric corrections. The significance of temporal change was assessed for two sites: the 'Degraded' site (a), and the nearby 'Reference' site (b). Based on columnar water variability observed with EPZ radiosondes (Fig. 3), along with empirically-derived atmospheric correction relationships for the ASTER thermal bands (Fig. 4), an expected range of Band 11 emissivities was computed from 1001 random samples per pixel. The simulation outcomes showed that the 3-year emissivity decrease at the 'Degraded' site was unaffected by modeling, with atmospheric profiles deviating by as much as 42% of columnar water vapor.

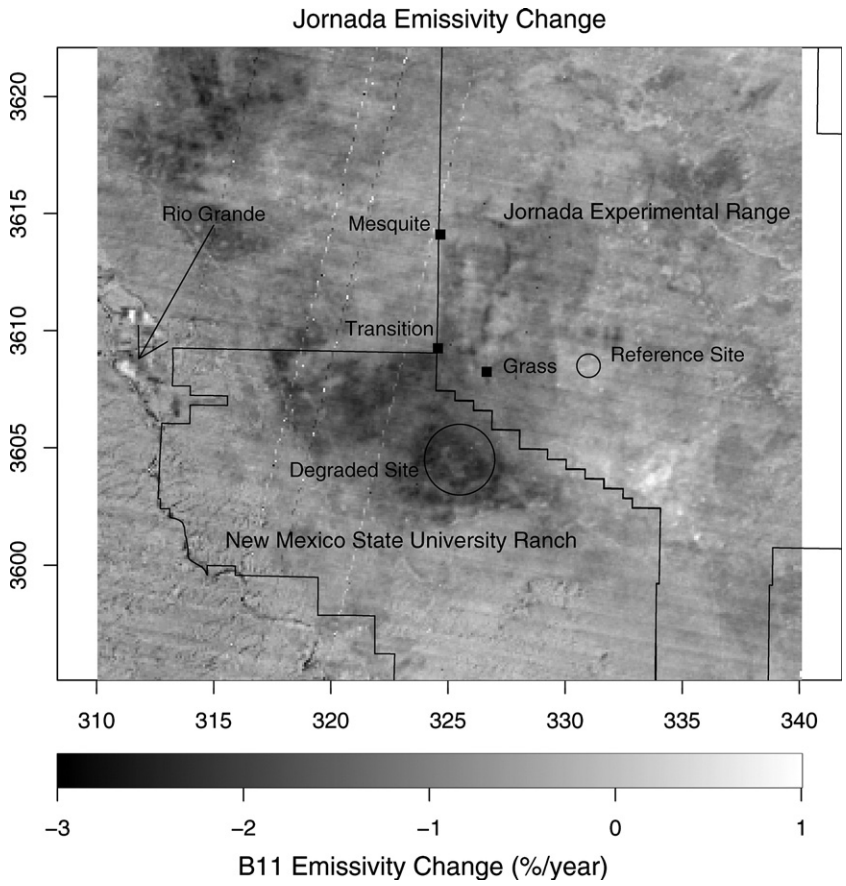

Fig. 6. Linear trend of ASTER band 11 emissivity decrease over Jornada study sites between February 2001 and October 2003. Scale is percent emissivity change per year. The most significant changes occur west and southwest of the Jornada Experimental Range boundary (indicated by the stair-step line). The three box symbols (north to south) indicate Mesquite, Transition, and Grass study sites. Northwest–southeast stripes, also seen in Fig. 7, are detector scan artifacts.

values for each term were then computed using the inverse of Eqs. (6) and (7). This approach accounts for differences between predicted and observed atmospheric transmissivities and path radiances. Using the columnar water variability estimated in step 1 as the standard error of mean water vapor, random values of apparent water vapor were generated to allow forward solutions of Eq. (6). Having simulated the atmospheric correction terms τ, $L\uparrow$, and $L\downarrow$, surface emissivities could be estimated from the NEM algorithm.

Lastly, in step four ASTER band 11 estimates for each pixel (1.05E9 of these) were consolidated for statistical analysis. Aggregation by target site resulted in data such as shown in Fig. 5, where ASTER band 11 emissivity quantiles are plotted for two sites spanning 2001–2003. Fig. 5 illustrates outcomes for two sites denoted as 'Degraded' and 'Reference'. These sites did not have ground observations and were selected for comparative purposes. The 'Degraded' site is the location of apparent land cover degradation and will be further discussed below. The 'Reference' site was chosen because it had no significant land cover change, as seen from remote sensing data. The site coincides with a fenced pasture having restricted access. In Fig. 5a, the temporal progression of ASTER band 11 emissivities are displayed for the 'Degraded' site. Fig. 5b displays the temporal progression for the nearby 'Reference' site, where emissivities showed less change. The symbols are conventional box and whisker displays of quantiles (1st quartile, median, 3rd quartile), except for the whiskers, which represent the full emissivity range. All 27 selected overpass times could be used for the 'Reference' site, but two fewer were used for the 'Degraded' site due to limited ASTER coverage for overpasses on 8 February and 7 November 2002. To estimate emissivity uncertainties caused by random errors in atmospheric corrections, linear trend lines were fit to data in each site. Detrending data for the 'Reference' site was statistically insignificant ($R^2=0.008$, $p<2.2E{-}16$). Residual error for the 'Degraded' site was 0.014, and for the 'Reference' site was 0.016, meaning that random atmospheric perturbations to NEM-derived Band 11 emissivities were $\leq 1.6\%$.

5. Observed temporal changes

Temporal change in land cover between 2001 and 2003 over Jornada was assessed in two ways: one in terms of change in land surface emissivities, and another in terms of change in NDVI. Although seasonal variations were likely embedded within the data series, only 3-year linear trends were considered because this was the simplest and least error-prone analysis possible. Modeling variations at higher orders would have placed greater demands on

accurate temporal sampling and would not allow suppression of erroneous short term (weekly to monthly) changes.

5.1. ASTER band 11 emissivity change

Considering the georegistered stack of 27 ASTER images, linear fits were computed for each pixel location by regressing band 11 emissivities against cumulative days since 1 January 2001. The resulting emissivity slope values (Fig. 6) ranged between −3% year^{-1} to +1% year^{-1}. For most of the Jornada region band 11 emissivity trends were small (<1%), suggesting no significant linear change in emissivity patterns occurred for this three year period. However, Fig. 6 also revealed spatially coherent regions – one of them ~5 km×10 km – near the southern and western boundaries of the USDA Jornada Range, where emissivities decreased by 2–3% year^{-1}. These decreases were greater than the 1.6% residual uncertainty estimated from the atmospheric simulation tests. A portion of this emissivity decrease region is delimited by the large black circle (repeated in Figs. 7 and 10). By comparison, a trapezoidal-shaped area (surrounding the small black circle indicating the 'Reference' site) showed negligible emissivity change. The explained variations of these emissivity changes are indicated in Fig. 7, which shows that the estimated linear trends have R^2 values up to 0.85 within the larger circled area. The trends were highly significant, with p values <2E10^{-16}. The extents of both the trend and the R^2 values, furthermore, were strongly correlated to land use patterns. Note for example the abrupt spatial termination of decreased emissivities along a roadway to the west and along rangeland boundaries to the north. These terminations could not have been caused by instrumental, processing, or atmospheric correction errors, meaning that the observed decreased emissivities were not data artifacts but were indicative of physical land cover changes corresponding to rangeland management practices.

These emissivity changes are consistent with retrieval algorithms other than NEM. To show this, the previously discussed 'Degraded' and 'Reference' sites were selected. Comparison of trends (Fig. 8) obtained from three different emissivity retrieval algorithms– NEM, TES, and TISI– showed similar linear trends for both sites. Shown in black are emissivities for the 'Degraded' site, and shown in gray are emissivities for the 'Reference' site. Absolute emissivity values from NEM, TES, and TISI significantly differed, despite use of identical remote sensing data and initial emissivities. However, the trend line slopes were similar, −2.09 to −2.70% year^{-1}, with R^2 values ranging 0.60 to 0.66 (Table 5). Slopes for the NEM and TISI emissivity trends were statistically identical and only slightly different from the TES trend. Standard errors for methods were also similar (~0.04% year^{-1}).

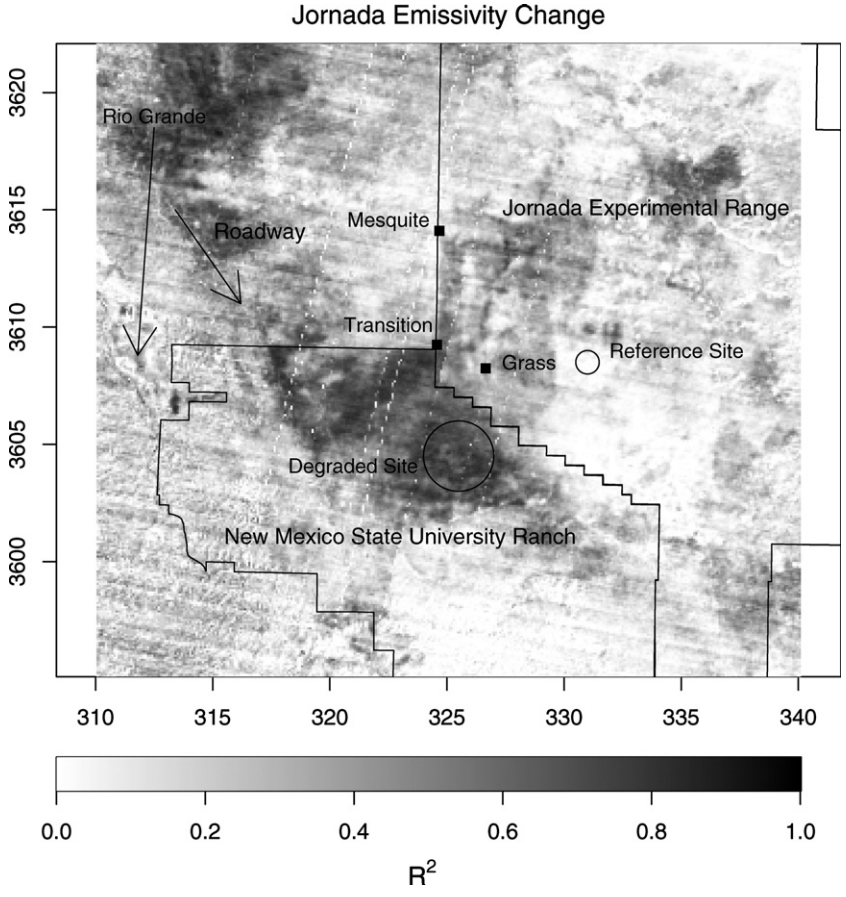

Fig. 7. Coefficient of determination (R^2) for linear trend of ASTER band 11 emissivity over Jornada study sites.

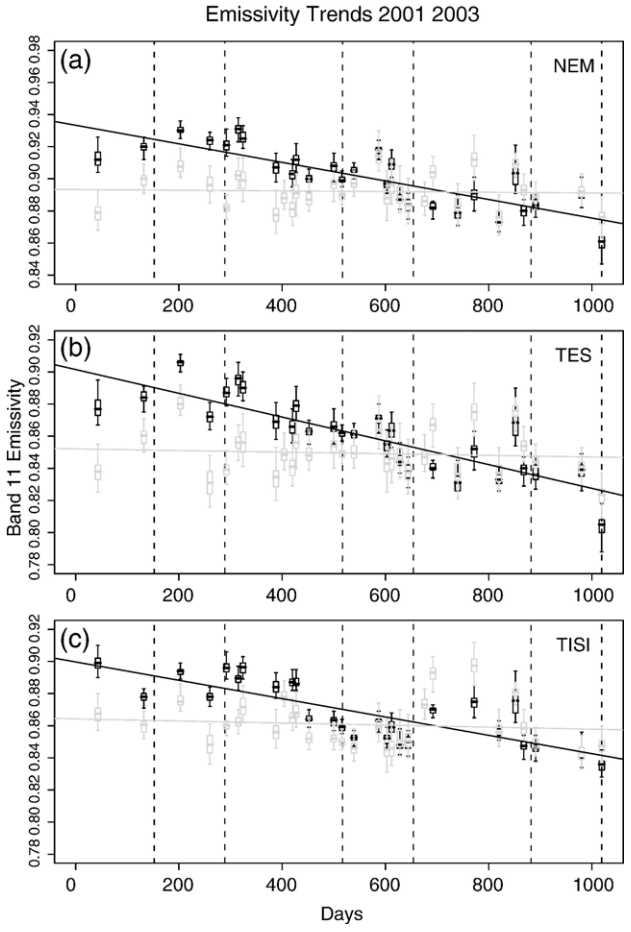

Fig. 8. Temporal emissivity trends over the 'Degraded' site (black) and the 'Reference' site (gray). Three different methods were used to estimate ASTER emissivities: NEM (a), TES (b), and TISI (c). All three methods show significant emissivity change for the 2001–2003 interval for the main site and no significant change for the reference site.

The significance of the coherent regions can also be tested by comparison against regions with no land cover change. One such region is White Sands, a ~20 km×25 km area covered by generally dry, unvegetated gypsum sand. Gypsum is an especially good stability test for ASTER band 11 due to its large potential sensitivity, ranging between 0.72 for a dry surface and 0.98 for a wet surface. Selecting a 12×20 pixel patch well within the White Sands area (1080 m×1800 m, 32.8348 N, 106.2925 W)[3] showed no significant emissivity change occurred over the 2001–2003 period (Fig. 9). Linear trend analysis for 9 scenes returned a slope of 0.3% year^{-1}, with R^2=0.02 and p value of 9.5E^{-15}.

5.2. MODIS band 29 emissivity change

The spatially coherent decreasing emissivity zones identified by ASTER are sufficiently large to compare with 1-km Terra MODIS observations. If sensors such as MODIS corroborate ASTER-based results, there will be not only the possibility of greatly expanded regional studies at 1 km resolution but also much more confidence that the changes are real and not instrumentation artifacts. MODIS has only three TIR bands comparable to ASTER's five (Fig. 2) but can still be analyzed with the NEM, TES or TISI approaches. For compatibility, the NEM approach was used for MODIS. The spectral band equivalent to ASTER band 11 is MODIS band 29 (Fig. 2), with the MODIS response weighted for slightly shorter wavelengths relative to ASTER band 11.

MODIS band 29 emissivity changes were estimated using the same 27 overpass days identified in Table 2. The resulting patterns (Fig. 10) are remarkable for their similarity to changes observed by ASTER (Fig. 6). Despite the coarser spatial resolution, band 29 emissivities from MODIS show the same 3% year^{-1} decrease within the 'Degraded' site (larger circle). Just as for the ASTER-based estimation, the MODIS emissivity trend within the 'Reference' site (smaller circle) showed no significant change over the 2001–2003 period. Five km eastward of the main region with decreasing emissivities lies a smaller region (with light gray tones) where emissivities increased by 1%. The same patch of increasing emissivity was observed by ASTER (Fig. 6).

5.3. ASTER NDVI change

Viewing Jornada from an NDVI perspective showed similar but less significant temporal changes than seen with emissivity (Fig. 11). Shown are trends for five sites: the 'Degraded' site, the 'Reference' site, and the three transect sites, Grass, Transition, and Mesquite. Plotted are NDVI quantiles for each site by elapsed days since 1 January 2001. The trendlines are least squares fits to the NDVI data over each site. The gray boxes approximate the extent of the monsoonal season, the most likely period for rainfall.

Visual inspection of trends suggested that NDVI decreased over time in the same way as it did for emissivity, including a weak suggestion of seasonally periodic changes. However, NDVI values at Jornada were usually low – ranging between 0.0 and 0.2 – and there was no apparent distinction in vegetation changes between the 'Degraded' and 'Reference' sites. Statistical analyses confirmed this observation. Unlike emissivity trends (Table 5), the NDVI linear trends were not significant (Table 6), with p values <2.2E−16. Considering standard errors, NDVI slopes for all five sites were indistinguishable. R^2 values were all negligible, meaning that NDVI changes over the three years could not be explained by linear trends.

To the extent that NDVI observations were correlative to vegetation cover, these results can be qualitatively checked by

Table 5
Emissivity trend estimation over the 'Degraded' site with NEM, TES, and TISI

Method	Slope (%/year)	Standard Error (%/year)	R^2
NEM	−2.09	0.036	0.63
TES	−2.70	0.043	0.66
TISI	−2.09	0.039	0.60

[3] ASTER resolution did not allow selecting the same site (Table 3) as used previously for ground samples because of mixed-pixel problems.

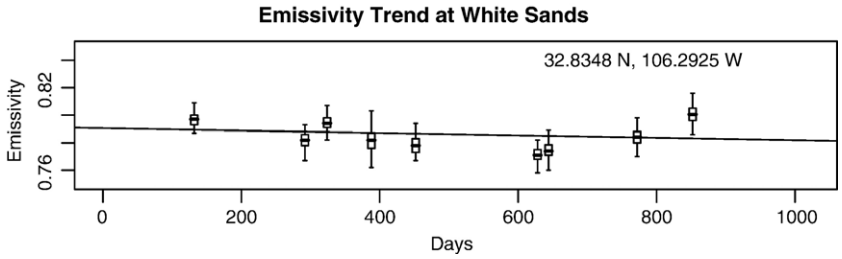

Fig. 9. ASTER Band 11 emissivity trend at White Sands, 2001–2003. A sample of 240 pixels from within the White Sands area (32.8348° N, 106.2925° W), showed no significant emissivity change over the three years, an outcome consistent with a bare, dry gypsum surface. Emissivities for Band 11 were retrieved within 1.1% uncertainty (residual error).

comparison against LAI transects collected at the Grass, Transition and Mesquite sites. The transects were important independent observations of vegetation cover, but unfortunately because of their locations and sampling frequencies, they could not be used in a rigorous way to confirm vegetation conditions in the 'Degraded' region. Fig. 12 summarizes the ground observations for 2001–2003. The 3-monthly rainfall bars at the base of the plot show that cumulative rainfall did not correspond to monsoon periods.

Generally, LAI values suggest a three-year decrease from 1.36 to 0.54–0.76 for the Grass and Transition sites. LAI values at the Mesquite site vary widely between 1.89 to 0.37, making trend assessment difficult. Site trends inferred by line segments are suggestive of decreasing LAI values at the Grass and Transition sites from May 2001 (Cumulative day 131) until October 2002 (Cumulative day 640). Causes for the anomalously low LAI data in September 2001 (Cumulative day 259) are unknown. These data were collected after unusually heavy rainfall and ponded water. With one exception for the Mesquite site, LAI values remained low (<0.68) from October 2002 until October 2003.

Explanation for the relatively poor discrimination ability of NDVI data may be provided by comparison against LAI transect data (Fig. 13). Plotted in the top figure are LAI vs.

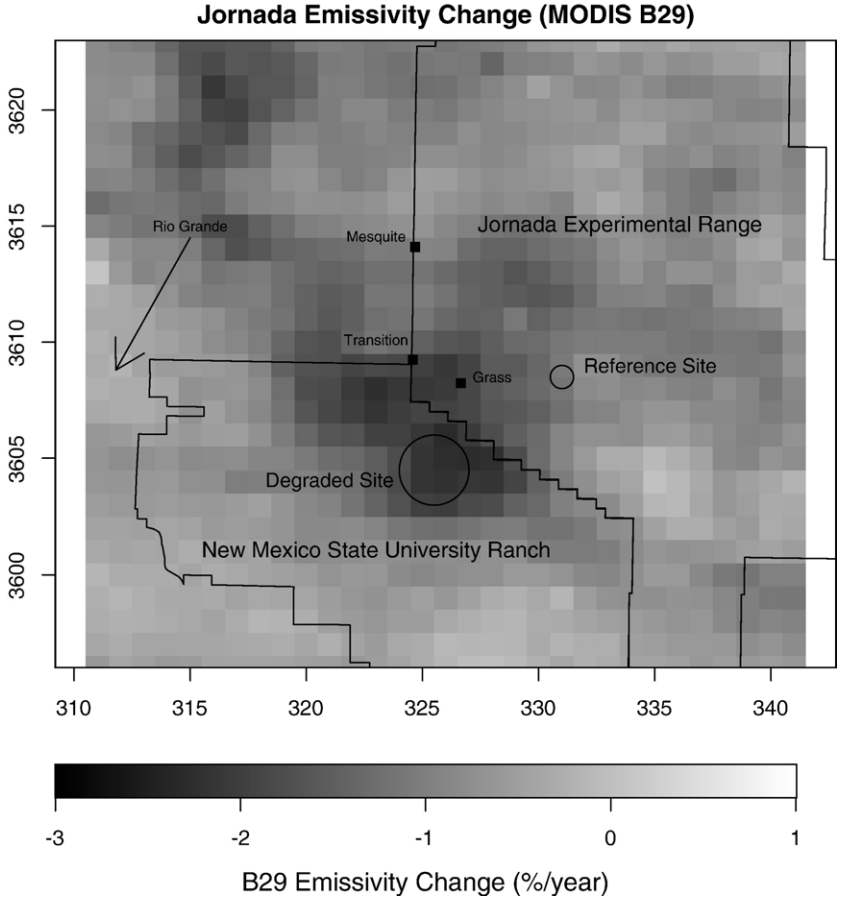

Fig. 10. Linear trend of MODIS band 29 emissivity over Jornada study sites between 2001 and 2003. Gray scale is the same as used in Fig. 6. MODIS data confirm the spatially coherent regions of decreasing emissivity west and south of Jornada.

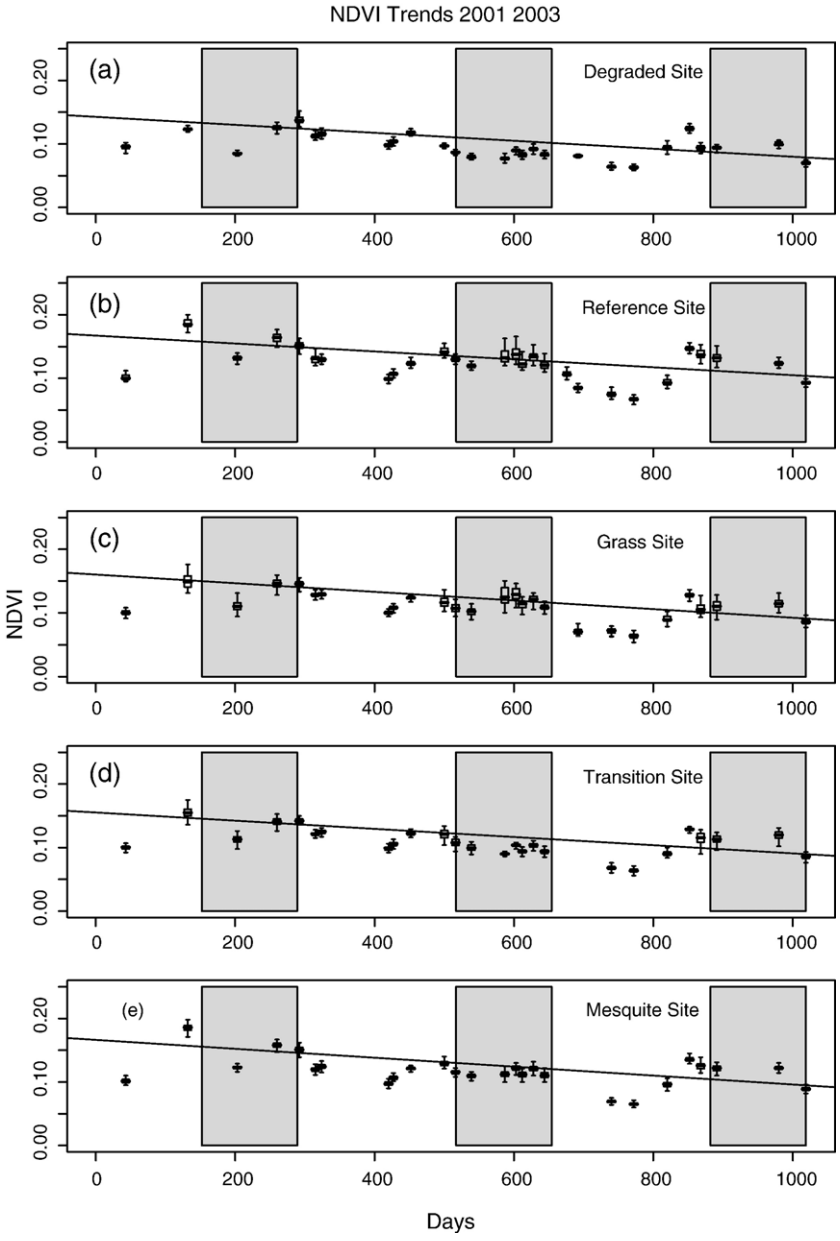

Fig. 11. NDVI temporal trends over five selected Jornada sites: the 'Degraded' site (a), the 'Reference' site (b), and the three LAI transect sites: Grass (c), Transition (d), and Mesquite (e). Shaded regions correspond to the monsoonal events evident in EPZ radiosonde profiles (Fig. 3).

ASTER band 11 emissivities, and plotted in the bottom figure are LAI vs. NDVI. For conditions ranging between bare soil and full cover, a linear-exponential relationship between LAI, emissivity, and NDVI could be expected, where asymptotes were reached for LAI values greater than ~3.0. For Jornada land cover conditions linear fits (indicated as solid lines) were sufficient because LAI values were less than 2.0. Six LAI transect observations were made, but one set made on 17 September 2001 was excluded (open symbols) because of very wet surface conditions. Such conditions affected all sites by increasing emissivities.

The relationship between LAI and NDVI agrees with the previous time series (Fig. 11) that showed trends with little distinction between sites. Statistical results (Table 7) show moderate to good explained variance (0.50–0.81). LAI/NDVI slope relationships were similar and agreed within standard errors.

Table 6
NDVI change statistics for five Jornada sites. Slope and standard error of slope shown as NDVI % year^{-1}

Site	Slope	Standard Error	Residual (%)	R^2
Degraded	−2.3	0.2	6.1	0.06
Reference	−2.3	0.2	5.8	0.07
Grass	−2.5	0.2	6.0	0.08
Transition	−2.3	0.2	6.0	0.07
Mesquite	−2.6	0.2	6.1	0.08

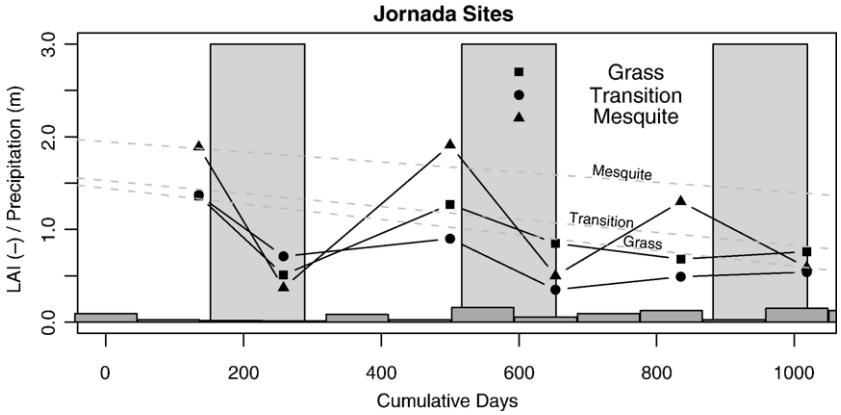

Fig. 12. Temporal LAI change at Jornada using 150 m ground transect data from 2001–2003. Solid lines connect transect observations while dashed lines are estimated LAI trends obtained from regressions shown in Fig. 13. Gray boxes approximate monsoonal seasons. Bars at bottom of plot are precipitation observations (m) aggregated over 3 month intervals.

The relationship between LAI and emissivity, on the other hand, suggests a stronger correlation exists for the sparse canopies at Jornada. Explained variance was good to excellent (0.81–0.99) for the three sites with significant discrimination between vegetation-emissivity slope relationships at the Mesquite site and the Transition and Grass sites (58.02 LAI/emissivity vs. 22.41 and 21.38). This discrimination is possibly related to spatial clumping of vegetation. At the Mesquite site, shrubs are strongly clumped with large bare soil expanses between dunes. At the Transition and Grass sites the vegetation is more uniformly distributed. A consequence of this clumping is that increases of LAI at the Mesquite site obscure significantly less soil than do increases at the other two sites. NDVI appears insensitive to clumping because the bulk of the canopies are non-green.

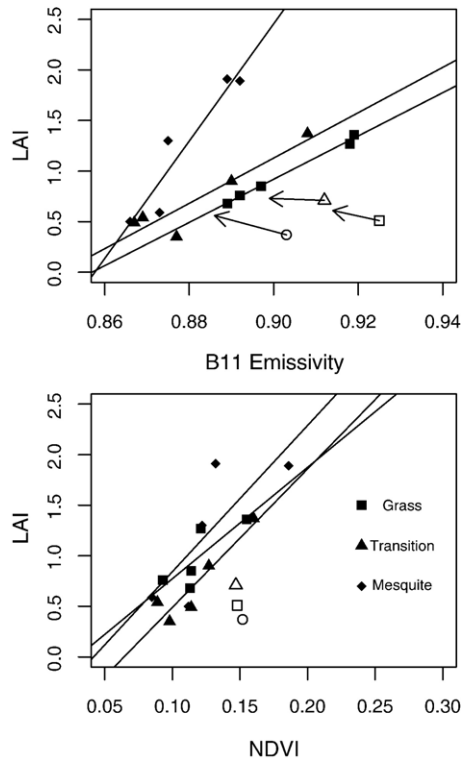

Fig. 13. LAI vs. B11 emissivity (top) and LAI vs. NDVI (bottom) for the Grass, Transition, and Mesquite transect sites. Plotted as solid symbols are averaged LAI values with their corresponding remote sensing observations for five different days: May 2001, May 2002, October 2002, April 2003, October 2003. Plotted as open symbols are values observed September 2001, made distinctive because of surface wet conditions. Regression lines (see Table 7) exclude this anomalous day and support good prediction of LAI from Band 11 emissivities but not from NDVI.

6. Emissivity–NDVI relationship

An issue not discussed so far is the relationship between emissivity and vegetation indices such as NDVI over arid landscapes. Some suggest a meaningful relationship between them exists (e.g., Van de Griend and Owe, 1993; Valor and Caselles, 1996; Bolle et al., 2006), meaning that difficult-to-obtain emissivity data could be replaced with much more available NDVI data. This substitution would be especially valuable because VNIR data also typically have greater spatial resolutions than possible with TIR data. The basis for the relationship is that surface emissivities are low over bare soils and high over vegetation canopies. Soil, when dry, often exhibits low emissivities (0.9 or less), while vegetation canopies are efficient scatterers and effectively blackbodies. Hence, as long as vegetation canopies are also photosynthetically active, vegetation indices should be able to track emissivity changes

Table 7
LAI regression statistics for Jornada sites with respect to ASTER band 11 emissivities (left) and ASTER NDVI (right)

Site	LAI vs. Emissivity			LAI vs. NDVI		
	Slope	R^2	Standard error	Slope	R^2	Standard error
Grass	21.38	0.99	1.01	11.01	0.52	4.73
Transition	22.41	0.81	5.22	13.70	0.81	3.19
Mesquite	58.02	0.86	11.53	14.46	0.50	6.46

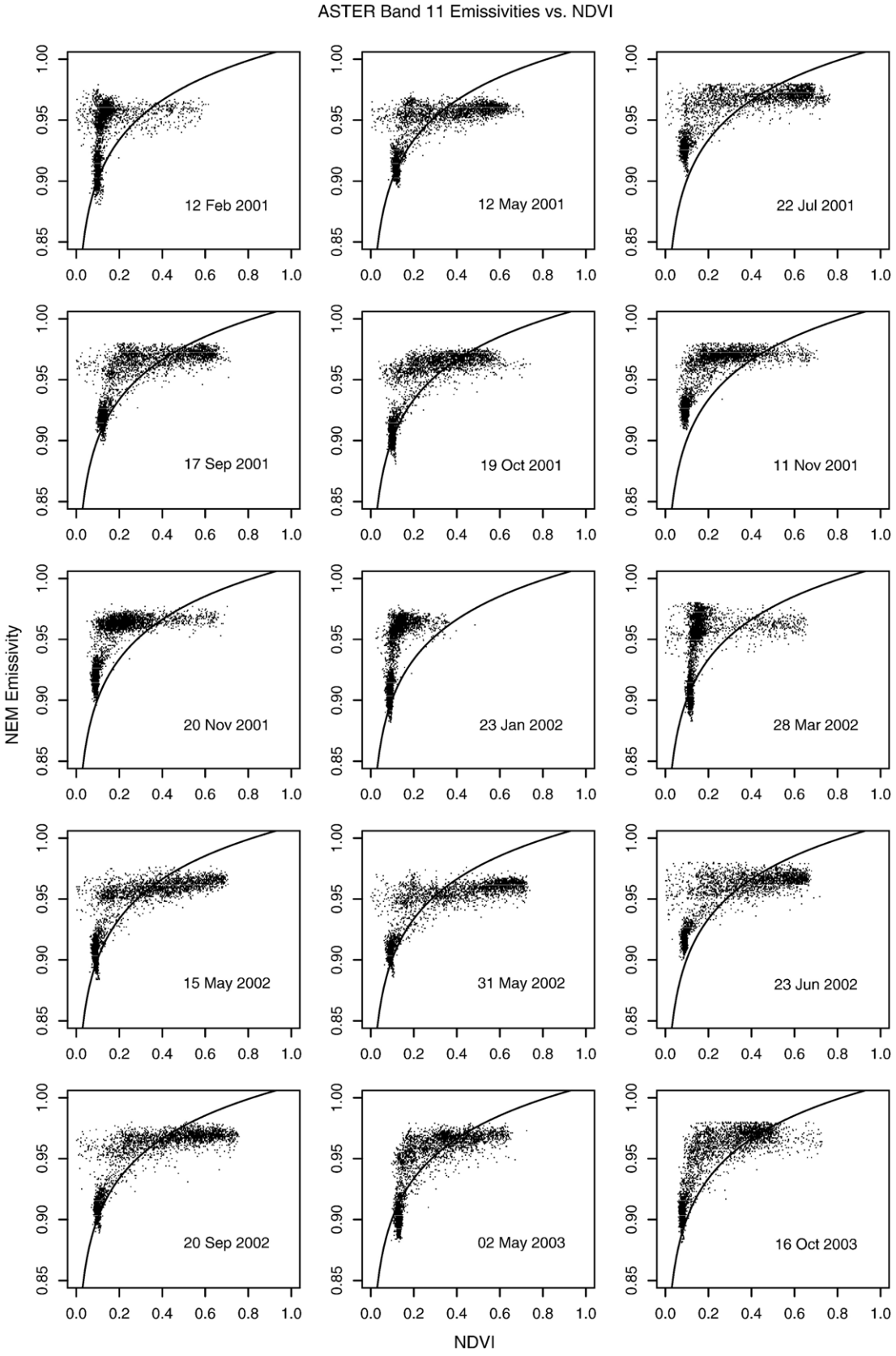

Fig. 14. ASTER Band 11 Emissivity vs. NDVI for mixed land cover in Las Cruces, NM. Each panel displays the relationship between emissivity in thermal band 11 (8.5–8.8 μm) and NDVI. Land cover types include bare soils, agricultural plots, water bodies, and urban land features. The solid line indicates an empirical broadband emissivity vs. NDVI relation (Van de Griend and Owe, 1993).

indirectly. Van de Griend and Owe (1993), for example, proposed a logarithmic formula relating broadband emissivity to ground-based NDVI observations based on calibrations over sites in Botswana:

$$\epsilon = 1.0094 + 0.047\ln(\mathrm{NDVI}) \quad (9)$$

Van de Griend and Owe (1993) suggest scale independence for the ϵ-NDVI relationship and demonstrate its use at satellite remote sensing scales. For longer wavelengths in the TIR window, 10.5–12.5 μm, Valor and Caselles (1996) show that by considering vegetation structure, modification of Eq. (9) allows its applicability to regions outside of Botswana. The question remains, however, how well models such as Eq. (9) could predict emissivities for land covered by sparse, dormant vegetation.

Using ASTER TIR and VNIR data from 15 different overpasses during 2001–2003 at Jornada (Fig. 14), the question can be partly answered. For this semi-arid landscape, dependence of ASTER Band 11 (8.475–8.825 μm) emissivity upon NDVI is in most instances questionable. With possible exceptions for scenes acquired after 15 May 2002, Band 11 emissivities are poorly correlated to NDVI, and there is a non-unique relationship for NDVI values between 0.1 and 0.2. For NDVI values less than 0.2, the slope of the scatter plots is essentially vertical, meaning there is no meaningful relationship between NDVI and spectral emissivities. For most dates displayed in Fig. 14, the maximum emissivity was nearly reached by NDVI ~0.2. The black curve (Eq. (9)), even if translated vertically, did not accurately represent observations, with emissivity discrepancies sometimes exceeding 3%.

Performing these analyses for broadband emissivities, instead of narrow band ones, likely would not substantively change these results (Gieske et al., 2004). Using a wider spectral interval would reduce the large emissivity variability seen at low NDVI while maintaining the flat response for higher NDVI. This lower variability may explain some of the success reported by Momeni and Saradjian (2007), who evaluated emissivities at 10.5–11.5 μm wavelengths at 1 km spatial resolution. In contrast, Jornada results show no reliable relationship between emissivity and NDVI exists at 90-m scales. While there could be ways to infer emissivities, using NDVI improved with geometrical parameters (Jiménez-Muñoz et al., 2006), the likelihood of its success in Jornada-like environments is poor because emissivity variability is not well-correlated to plant greenness.

7. Discussion

Retrieval and analysis of ASTER TIR data over southern New Mexico rangeland shows strong, consistent, and coherent regions of decreasing band 11 emissivities over the three-year period, indicating that land cover change for this environment can be monitored from space. ASTER thermal infrared observations over the Jornada Experimental Range and the adjacent New Mexico State University Ranch have revealed patches of land, ~5 km × 10 km, where emissivities at 8.6 μm decreased on the order of 3% year^{-1}, with early 2001 NEM-based emissivities of ~0.93 decreasing to ~0.87 by late 2003.

We interpret these patches as areas of decreased vegetation densities where sparsely vegetated land were further degraded, exposing greater amounts of bare soil over a three year period. What is notable for the emissivity data is not the short term, seasonal changes in vegetation – these might be observed in a better way using VI data – but rather the inter-annual changes regardless of seasonality. The physical reason for this difference is explained by the dynamics of rangeland vegetation and the fact that VI and emissivity observations respond to different biochemical and structural properties of vegetation. VI responds to plant chlorophyll densities, while emissivity responds to plant canopy geometry and patterns between plant canopies. This difference in response was described in Section 6. Since VI changes are seasonal according to plant growth cycles, their variability within a year is just as large as between years, which means that it can be difficult to distinguish long-term change from short-term changes. This difficulty has been noted by others (e.g., Li et al., 2005).

Emissivity changes, on the other hand, are less likely to show such seasonal variability over persistent vegetation because the multi-scattering effects result from plant matter regardless of chlorophyll content. At time scales greater than a year, plant distributional patterns do change, and in these cases corresponding emissivities changes can be detected. Hence, emissivity variabilities within a year (absent surface wetting events) are small, while variabilities between years could be large. To illustrate how the land cover change could be estimated, the regression results from comparing LAI transect data to band 11 emissivities (Table 7) were applied to the entire collection of 27 ASTER scenes and plotted as dashed gray lines in Fig. 12. The tentative trends (i.e., regression results were based on too few observations to warrant greater certainty) show how LAI values at the Mesquite site may have decreased from ~2.0 to 1.3 between 2001 and 2003. For the Transition and Grass sites, the decrease appears to be from 1.5 to 0.8.

Alternative interpretations of the Jornada emissivity patterns were also considered, such as the possibility of data collection and processing artifacts. These included TIR calibration errors, detector degradation, and inaccurate atmospheric corrections, none of which could be reconciled with all observations. TIR calibration and detector problems were unlikely because the ASTER gains were episodically monitored and updated to reflect correct gains and offsets. Poor atmospheric corrections, though certainly a concern, were demonstrated to potentially cause emissivity errors no greater than 1.6%. Furthermore, the correction errors from radiosonde profiles would not cause systematic trends, nor would such errors induce the discrete and the well-delineated patches evident in Fig. 6.

Another interpretation is that the emissivity changes were due to changes in soil emissivity. These could be induced by various factors such as change in surface organic matter, surface texture, and surface moisture. Soil emissivities in particular have some dependency upon surface grain size (e.g., Salisbury and Eastes, 1985). It is plausible – though in this instance unverifiable – that the observed emissivity changes were related

to grazing activity which may have disturbed the surface soil texture. Soil emissivity changes can also be seen with changing surface moisture, but in these cases the changes occur over short time spans, such as observed for the September 17, 2002 overpass.

Considering that these alternatives were either unlikely or conjectural, the more probable explanation for the three-year emissivity patterns, whether decreasing or increasing, is due to change in vegetation canopy densities. For sparsely vegetated terrain, the interaction between high-emissivity vegetation and low-emissivity soils explains in a physically meaningful way the spatial and temporal distribution of observed emissivity patches. As vegetation densities increase, low emissivity surfaces are increasingly masked by higher emissivity surfaces. There is also evidence from ground transect data that the temporal emissivity decrease is associated with LAI decreases at three peripheral sites (Fig. 12 and Table 7). With two exceptions, canopy LAI values at the Grass, Transition, and Mesquite sites dropped from ~1.4 to ~0.6, a change of more than 50%. The environmental causes for the vegetation density changes are unknown and apparently are not linked to short term precipitation patterns (Fig. 12).

8. Conclusions

Detection of land cover change is an important role for remote sensing whereby long-term observations can be used to monitor spatial and temporal seasonal to multi-year patterns in vegetation cover. The usual approach to this task is to construct VI maps, derived from normalized red and near infrared data. Generally these maps have good quality and are extremely valuable for tracking seasonal vegetation changes. Nevertheless, VI techniques distinguish non-green vegetation from background soils with difficulty, which means that signals from long term changes can be overwhelmed by seasonal effects. Such circumstances commonly arise for both cultivated and uncultivated lands.

In this study we have shown a complementary approach that may improve abilities to discriminate vegetation cover regardless of plant color. Using thermal infrared observations from a one-of-a-kind remote sensing instrument, ASTER, seasonal land cover changes can be detected by using spectral emissivities. Unlike VI data, TIR emissivity data respond to changes in vegetation canopy densities and to changes in surface soil properties. Provided that the emissivity for soil is significantly different from vegetation, emissivity changes over time can be detected. When viewed at multi-year time scales, long-term changes in land cover, not otherwise recognized, can be mapped spatially at 100-m scales.

Analysis of 27 ASTER scenes over the Jornada Experimental Range between 2001–2003 revealed spatially coherent land cover patterns with decreasing band 11 emissivities. At these locales, emissivities declined at the rate of ~3% year^{-1} with high confidence (R^2 values up to 0.82). The identification of these regions, corroborated by 1 km MODIS TIR data, supports ground-based LAI observations where cover decreased from over 1.0 to ~0.7. Comparable NDVI observations showed similar decreases at all sites, but the linear trends were indistinguishable and statistically insignificant.

These results highlight the importance of multispectral thermal infrared data that includes observations at wavelengths within 8–9.5 μm. The value of TIR data extends beyond land surface temperature retrieval to include the information rich portion of the TIR window. Commonly, TIR detectors sample TIR data at wavelengths between 10–13.5 μm for split window analyses. For land surface applications, variability of surface emissivities at these wavelengths is typically small and difficult to use for change assessment in the manner described in this study. A TIR remote sensing strategy that is better for both temperature and emissivity estimation is to include observations within the 8–9.5 μm interval, where emissivity variations due to soils and vegetation are frequently large. These data, in combination with longer wavelength TIR data, will provide valuable land cover information unavailable using other remote sensing bands. Future work will expand the emissivity change assessment to more sites throughout the U.S. Southwest.

Acknowledgments

This work was supported in part by NASA EOS Grant 03-OES-02 and by the USDA/ARS Jornada Experimental Station. The laboratory soil sample measurements were made by Cindy Grove, Jet Propulsion Laboratory, California Institute of Technology, Pasadena, California. Data analysis and presentation were greatly facilitated by using the R package (R Development Core Team, 2006). Precipitation data were provided by the Jornada Long-Term Ecological Research (LTER) project and were funded by the U.S. National Science Foundation (Grant DEB-92-40261).

References

Anyamba, A., & Eastman, J. (1996). Interannual variability of NDVI over Africa and its relation to El Niño/Southern Oscillation. *International Journal of Remote Sensing*, *17*(13), 2533–2548.

Bannari, A., Pacheco, A., Staenz, K., McNairn, H., & Omari, K. (2006). Estimating and mapping crop residues cover on agricultural lands using hyperspectral and IKONOS data. *Remote Sensing of Environment*, *104*(4), 447–459.

Baret, F., Clevers, J., & Steven, M. (1995). The robustness of canopy gap fraction estimates from red and near-infrared reflectances: A comparison of approaches. *Remote Sensing of Environment*, *54*, 141–151.

Becker, F., & Li, Z. -L. (1990). Temperature-independent spectral indices in thermal infrared bands. *Remote Sensing of Environment*, *32*, 17–33.

Bolle, H. -J., Eckardt, M., Koslowsky, D., Maselli, F., Miralles, J. M., Menenti, M., Olesen, F. -S., Pekov, L., Rasool, I., & de Griend, A. V. (Eds.), (2006). *Meditteranean land-surface processes assessed from space* (pp. 257–265). Springer chapter 5.

Buffington, L., & Herbel, C. (1965). Vegetational changes on a semidesert grassland range from 1853 to 1963. *Ecological Monographs*, *35*, 139–164.

Byrne, P., Crapper, P., & Mayo, K. (1980). Monitoring land-cover change by principal component analysis of multitemporal Landsat data. *Remote Sensing of Environment*, *10*, 175–184.

Carlson, T., & Ripley, D. (1997). On the relation between NDVI, fractional vegetation cover, and leaf area index. *Remote Sensing of Environment*, *62*, 241–252.

Chehbouni, A., Goodrich, D., Moran, M., Watts, C., Kerr, Y., Dedieu, G., Kepner, W., Shuttleworth, W., & Sorooshian, S. (2000). A preliminary

synthesis of major scientific results during the SALSA program. *Agricultural and Forest Meteorology*, *105*, 311−323.

Choudhury, B. J. (1987). Relationships between vegetation indices, radiation absorption, and net photosynthesis evaluated by a sensitivity analysis. *Remote Sensing of Environment*, *22*, 209−233.

Dash, P., Göttsche, F. -M., Olesen, F. -S., & Fischer, H. (2002). Land surface temperature and emissivity estimation from passive sensor data: Theory and practice-current trends. *International Journal of Remote Sensing*, *23*(13), 2563−2594.

Dash, P., Göttsche, F. -M., Olesen, F. -S., & Fischer, H. (2005). Separating surface emissivity and temperature using two-channel spectral indices and emissivity composites and comparison with a vegetation fraction method. *Remote Sensing of Environment*, *96*, 1−17.

Daughtry, C., Hunt, E. R., Jr., Doraiswamy, P., & McMurtrey, J. (2005). Remote sensing the spatial distribution of crop residues. *Agronomy Journal*, *97*(3), 864−871.

Dial, G., Bowen, H., Gerlach, F., Grodecki, J., & Oleszczuk, R. (2003). IKONOS satellite, imagery, and products. *Remote Sensing of Environment*, *88*(1–2), 23−36.

Diouf, A., & Lambin, E. (2001). Monitoring land-cover changes in semi-arid regions: remote sensing data and field observations in the Ferlo, Senegal. *Journal of Arid Environments*, *48*(2), 129−148.

El Kharraz, J., Sobrino, J. A., Morales, L., Jiménez-Muñoz, J. C., Sória, G., Gómez, M., & Romaguera, M. (2004). Land cover dynamic analysis over the Mediterranean basin by means of remotely sensed and climate data. *Proceedings of SPIE-The International Society for Optical Engineering*, *5232*, 627−634.

Elvidge, C. D. (1988). Thermal infrared reflectance of dry plant materials: 2.5–20.0 μm. *Remote Sensing of Environment*, *26*, 265−285.

Falkenmark, M. (1997). Meeting water requirements of an expanding world population. *Philosophical Transactions of the Royal Society. Series B: Biological Sciences*, *352*(1356), 929−936.

Fang, H. (1998). Rice crop area estimation of an administrative division in China using remote sensing data. *International Journal of Remote Sensing*, *19*(17), 3411−3419.

French, A., Schmugge, T., & Kustas, W. (2000). Discrimination of senescent vegetation using thermal emissivity contrast. *Remote Sensing of Environment*, *74*, 249−254.

Fuchs, M., & Tanner, C. (1966). Infrared thermometry of vegetation. *Agronomy Journal*, *58*, 597−601.

Fuchs, M., & Tanner, C. (1968). Surface temperature measurements of bare soils. *Journal of Applied Meteorology*, *7*, 303−305.

Gibbens, R., McNeely, R., Havstad, K., Beck, R., & Nolen, B. (2006). Vegetation changes in the Jornada Basin from 1858 to 1998. *Journal of Arid Environments*, *61*, 651−668.

Gieske, A. S., Wubett, M. T., Timmermans, W. J., Parodi, G. N., Wolski, P., & Arneth, A. (2004). Temperature-emissivity separation with ASTER and LANDSAT 7 imagery validation on the fringe of the Okavango Delta, Botswana. In M. Owe, G. D'Urso, J. F. Moreno, & A. Calera (Eds.). *Remote Sensing for Agriculture, Ecosystems, and Hydrology V, Proceedings of the SPIE*, *vol. 5232*. (pp. 489−498).

Gillespie, A. 1985. Lithologic mapping of silicate rocks using TIMS, The TIMS data users' workshop, Technical report, Jet Propulsion Laboratory. JPL Publication 86–38, pp. 29–44.

Gillespie, A., Rokugawa, S., Matsunaga, T., Cothern, J., Hook, S., & Kahle, A. (1998). A temperature and emissivity separation algorithm for advanced spaceborne thermal emission and reflection radiometer (ASTER) images. *IEEE Transactions on Geoscience and Remote Sensing*, *36*, 1113−1126.

Goward, S., Masek, J., Williams, D., Irons, J., & Thompson, R. (2001). The Landsat 7 mission — Terrestrial research and applications for the 21st century. *Remote Sensing of Environment*, *78*, 3−12.

Gutman, G., & Ignatov, A. (1998). The derivation of green vegetation fraction from NOAA/AVHRR data for use in numerical weather prediction models. *International Journal of Remote Sensing*, *19*, 1533−1543.

Havstad, K., Kustas, W., Rango, A., Ritchie, J., & Schmugge, T. (2000). Jornada Experimental Range: A unique arid land location for experiments to validate satellite systems. *Remote Sensing of Environment*, *74*(1), 13−25.

Hook, S., Dmochowski, J., Howard, K., Rowan, L., Karlstrom, K., & Stock, J. (2005). Mapping variations in weight percent silica measured from multispectral thermal infrared imagery — Examples from the Hiller Mountains, Nevada, USA and Tres Virgenes–La Reforma, Baja California Sur, Mexico. *Remote Sensing of Environment*, *95*, 273−289.

Hook, S. J., Gabell, A., Green, A., & Kealy, P. (1992). A comparison of techniques for extracting emissivity information from thermal infrared data for geologic studies. *Remote Sensing of Environment*, *42*, 123−135.

Hook, S. J., Meyers, J. J., Thome, K. J., Fitzgerald, M., & Kahle, A. B. (2001). The MODIS/ASTER airborne simulator (MASTER) — A new instrument for earth science studies. *Remote Sensing of Environment*, *76*, 93−102.

Humes, K., Kustas, W., Moran, M., Nichols, W., & Weltz, M. (1994). Variability of emissivity and surface temperature over a sparsely vegetated surface. *Water Resources Research*, *30*(5), 1299−1310.

Jacob, F., Petitcolin, F., Schmugge, T., Vermote, E., Ogawa, K., & French, A. (2004). Comparison of land surface emissivity and radiometric temperature from MODIS and ASTER sensors. *Remote Sensing of Environment*, *83*, 1−18.

Jacob, F., Schmugge, T., Olioso, A., French, A., Courault, D., Ogawa, K., Petitcolin, F., Chehbouni, G., Pinheiro, A., Privette, J. (in press). Potential of thermal infrared remote sensing for the monitoring of land surface processes. In S. Liang (Ed.). *Advances in Land Remote Sensing: System, Modeling, Inversion and Application*. Chapter 10, Springer.

Jet Propulsion Laboratory (2001). *ASTER spectral library.* http://speclib.jpl.nasa.gov

Jiang, Z., Huete, A. R., Chen, J., Chen, Y., Li, J., Yan, G., & Zhang, X. (2006). Analysis of NDVI and scaled difference vegetation index retrievals of vegetation fraction. *Remote Sensing of Environment*, *101*(3), 366−378.

Jiménez-Muñoz, J. C., Sobrino, J. A., Gillespie, A., Sabol, D., & Gustafson, W. T. (2006). Improved land surface emissivities over agricultural areas using ASTER NDVI. *Remote Sensing of Environment*, *103*, 474−487.

Justice, C., Holben, B., & Gwynne, M. (1986). Monitoring East African vegetation using AVHRR data. *International Journal of Remote Sensing*, *7*(11), 1453−1474.

Justice, C., & Townshend, J. (2002). Special issue on the moderate resolution imaging spectroradiometer (MODIS): A new generation of land surface monitoring. *Remote Sensing of Environment*, *83*(1–2), 1−2.

Justice, C., Vermote, E., Townshend, J., Defries, R., Roy, D., Hall, D., Salomonson, V., Privette, J., Riggs, G., Strahler, A., Lucht, W., Myneni, R., Knyazikhin, Y., Running, S., Nemani, R., Wan, Z., Huete, A., Leeuwen, W., Wolfe, R., Giglio, L., Muller, J. -P., Lewis, P., & Barnsley, M. (1998). The MODerate Imaging Spectroradiometer (MODIS): Land remote sensing for global change research. *IEEE Transactions on Geoscience and Remote Sensing*, *36*, 1228−1249.

Kahle, A. B., & Alley, R. E. (1992). Separation of temperature and emittance in remotely sensed radiance measurements. *Remote Sensing of Environment*, *42*, 107−111.

Kahle, A., Madura, D., & Soha, J. (1980). Middle infrared multispectral aircraft scanner data: analysis for geologic applications. *Applied Optics*, *19*, 2279−2290.

Li, Y., Chen, J., Gong, P., & Yue, T. (2005). Study on land cover change detection method based on NDVI time series datasets: Change detection indexes design. *Journal of Basic Science and Engineering*, *13*(3), 261−275.

Li, Z. -L., Becker, F., Stoll, M., & Wan, Z. (1999). Evaluation of six methods for extracting relative emissivity spectra from thermal infrared images. *Remote Sensing of Environment*, *69*, 197−214.

Matsunaga, T. (1994). A temperature-emissivity separation method using an empirical relationship between the mean, the maximum, and the minimum of the thermal emissivity spectrum. *Journal of Remote Sensing Society Japan*, *14*(2), 230−241. in Japanese with English abstract.

Menenti, M., Jia, L., & Bastiaanssen, W. (2005). Energy and water flow through the soil–vegetation–atmosphere system: the fiction of measurements and the reality of models. In R. Feddes, G. Rooij, & J. van Dam (Eds.). *Papers for the Frontis workshop on unsaturated-zone modeling: progress, challenges and applications, Wageningen, The Netherlands 3–5 October 2004* (pp. 211−229). Springer.

Momeni, M., & Saradjian, M. (2007). Evaluating NDVI-based emissivities of MODIS bands 31 and 32 using emissivities derived by Day/Night LST algorithm. *Remote Sensing of Environment*, *106*(2), 190−198.

Mushkin, A., Balick, L. K., & Gillespie, A. R. (2005). Extending surface temperature and emissivity retrieval to the mid-infrared (3–5 μm) using the Multispectral Thermal Imager (MTI). *Remote Sensing of Environment*, *98*, 141−151.

Nerry, F., Petitcolin, F., & Stoll, M. (1998). Bidirectional reflectivity in AVHRR channel 3: application to a region in northern Africa. *Remote Sensing of Environment*, *66*, 298−316.

Norman, J., Divakarla, M., & Goel, N. (1995). Algorithms for extracting information from remote thermal-IR observations of the earth's surface. *Remote Sensing of Environment*, *51*, 157−168.

Norman, J. M., & Becker, F. (1995). Terminology in thermal infrared remote sensing of natural surfaces. *Agricultural and Forest Meteorology*, *77*, 153−166.

Palluconi, F., Kahle, A., Hoover, G., & Conel, J. (1990). *The spectral emissivity of prairie and pasture grasses at Konza prairie, Kansas. Proc. Amer. Meteorol. Soc. Symp. on the First ISLSCP Field Experiment (FIFE) Feb. 7–9*, *Vol. 45*. Beacon St., Boston, MA USA: American Meteorological Society.

Pelgrum, H. (2000). Length-scale analysis of surface albedo, temperature, and normalized difference vegetation index in desert grassland. *Water Resources Research*, *36*(7), 1757−1765.

Petitcolin, F., & Vermote, E. (2002). Land surface reflectance, emissivity and temperature from MODIS middle and thermal infrared data. *Remote Sensing of Environment*, *83*(1–2), 112−134.

Qi, J., Chehbouni, A., Huete, A., Kerr, Y., & Sorooshian, S. (1994). A modified soil adjusted vegetation index. *Remote Sensing of Environment*, *48*, 119−126.

R Development Core Team (2006). R: A language and environment for statistical computing. *R Foundation for Statistical Computing, Vienna, Austria.* ISBN 3-900051-07-0.URL: http://www.R-project.org

Rango, A., Huenneke, L., Buonopane, M., Herrick, J., & Havstad, K. (2005). Using historic data to assess effectiveness of shrub removal in southern New Mexico. *Journal of Arid Environments*, *62*, 75−91.

Rowan, L., & Mars, J. (2003). Lithologic mapping in the Mountain Pass, California area using Advanced Spaceborne Thermal Emission and Reflection Radiometer (ASTER) data. *Remote Sensing of Environment*, *84*, 350−366.

Rowan, L., Mars, J., & Simpson, C. (2005). Lithologic mapping of the Mordor, NT, Australia ultramafic complex by using the Advanced Spaceborne Thermal Emission and Reflection Radiometer (ASTER). *Remote Sensing of Environment*, *99*(1–2), 105−126.

Salisbury, J. W., & D'Aria, D. M. (1992). Emissivity of terrestrial materials in the 8–14 μm atmospheric window. *Remote Sensing of Environment*, *42*, 83−106.

Salisbury, J. W., & Eastes, J. W. (1985). The effect of particle size and porosity on spectral contrast in the mid-infrared. *Icarus*, *64*, 586−588.

Snyder, K., & Tartowski, S. (2006). Multi-scale temporal variation in water availability: implications for vegetation dynamics in arid and semi-arid ecosystems. *Journal of Arid Environments*, *65*, 219−234.

Su, Z. B. (2000). Remote sensing of land use and vegetation for mesoscale hydrological studies. *International Journal of Remote Sensing*, *21*(2), 213−233.

Sutherland, R., & Bartholic, J. (1977). Significance of vegetation in interpreting thermal radiation from a terrestrial surface. *Journal of Applied Meteorology*, *16*, 759−763.

Telesca, L., & Lasaponara, R. (2006). Quantifying intra-annual persistent behaviour in SPOT-VEGETATION NDVI data for Mediterranean ecosystems of southern Italy. *Remote Sensing of Environment*, *101*, 95−103.

Tonooka, H. (2001). An atmospheric correction algorithm for thermal infrared multispectral data over land — A water-vapor scaling method. *IEEE Transactions on Geoscience and Remote Sensing*, *39*(3), 682−692.

Tonooka, H., Palluconi, F., Hook, S., & Matsunaga, T. (2005). Vicarious calibration of ASTER thermal infrared bands. *IEEE Transactions on Geoscience and Remote Sensing*, *43*, 2733−2746.

Tonooka, H., Sakuma, F., Kudoh, M., & Iwafune, K. (2003). ASTER/TIR calibration status and user-based recalibration. *Proceedings of SPIE*, *vol. 5234*. (pp. 191−201): SPIE.

Valor, E., & Caselles, V. (1996). Mapping land surface emissivity from NDVI: application to European, African, and South American areas. *Remote Sensing of Environment*, *57*, 167−184.

Van de Griend, A., & Owe, M. (1993). On the relationship between thermal emissivity and the normalized difference vegetation index for natural surfaces. *International Journal of Remote Sensing*, *14*(6), 1119−1131.

Vermote, E. F., Tanré, D., Deuzé, J. L., Herman, M., & Morcrette, J. -J. (1997). Second simulation of the satellite signal in the solar spectrum, 6S: and overview. *IEEE Transactions on Geoscience and Remote Sensing*, *35*(3), 675−686.

Wardlow, B. D., Egbert, S. L., & Kastens, J. H. (2007). Analysis of timeseries MODIS 250 m vegetation index data for crop classification in the U.S. Central Great Plains. *Remote Sensing of Environment*, *108*(3), 290−310.

Watson, K. (1992). Two-temperature method for measuring emissivity. *Remote Sensing of Environment*, *42*, 117−121.

Yamaguchi, Y., Kahle, A., Tsu, H., Kawakami, T., & Pniel, M. (1998). Overview of advanced space-borne thermal emission and reflection radiometer (ASTER). *IEEE Transactions on Geoscience and Remote Sensing*, *36*, 1282−1289.

Zhang, H. -Y., & Smith, W. (1990). The spectral variation of surface emissivity within the 8–12 μm "window". *Proceedings of the Fall American Geophysical. Union Meeting* 2000 Florida Ave., NW, Washington, DC 20009 USA: American Geophysical Union.